Applied Surface Science 403 (2017) 282–293

Contents lists available at ScienceDirect

Applied Surface Science

journal homepage: www.elsevier.com/locate/apsusc

Full length article

γ-Irradiation assisted synthesis of graphene oxide sheets supported Ag nanoparticles with single crystalline structure and parabolic distribution from interlamellar limitation

Yunhao Yue [1], Baoming Zhou [1], Jie Shi, Cheng Chen, Nan Li, Zhiwei Xu *, Liangsen Liu, Liyun Kuang, Meijun Ma, Hongjun Fu

State Key Laboratory of Separation Membranes and Membrane Processes, School of Textiles, Tianjin Polytechnic University, Tianjin 300387, China

ARTICLE INFO

Article history:
Received 8 September 2016
Received in revised form 15 January 2017
Accepted 16 January 2017
Available online 19 January 2017

Keywords:
Silver nanoparticles
Graphene oxide sheets
Interlamellar limitation
γ-Irradiation
Surface-enhanced Raman scattering

ABSTRACT

This paper reported a method to fabricate graphene oxide sheets supported Ag nanoparticles (AgNPs/GOS) with single crystalline structure and parabolic distribution without surfactant or functional agent. We used imidazole silver nitrate as intercalation precursor into the layers of graphite oxide, and subsequently reduction and growth of interlamellar AgNPs were induced via γ-irradiation. The results illustrated that the synergism of interlamellar limitation of graphite oxide and fragmentation ability of γ-irradiation could prevent coalescent reaction of AgNPs with other oligomeric clusters, and the single crystalline and small-sized (below 13.9 nm) AgNPs were prepared. Moreover, the content and size of AgNPs exhibited parabolic distribution on GOS surface because the graphite oxide exfoliated to GOS from the edge to the central area of layers. In addition, complete exfoliation degree of GOS and large-sized AgNPs were obtained simultaneously under suitable silver ions concentration. Optimized composites exhibited outstanding surface-enhanced Raman scattering properties for crystal violet with enhancement factor of 1.3×10^6 and detection limit of 1.0×10^{-7} M, indicating that the AgNPs/GOS composites could be applied to trace detection of organic dyes molecules. Therefore, this study presented a strategy for developing GOS supported nanometal with single crystalline structure and parabolic distribution based on γ-irradiation.

1. Introduction

Noble metal nanoparticles are consistently investigated worldwide because of their outstanding physical and chemical properties [1,2]. Silver nanoparticles (AgNPs) are a well-known noble nanometal of current interest with remarkable optical properties, high electrical conductivity and excellent catalytic activity, etc. Based on these outstanding properties, AgNPs are effective in various applications, including surface-enhanced Raman scattering (SERS) substrate, oxidative catalysis, antimicrobial medicine and optical sensors, etc. [3–16]. As is well known, the SERS activity and stability of AgNPs depend on distribution and crystalline structure. The appropriate interparticle gap is suitable for the generation of Raman "hot spots", which is conducive to enhancing the SERS properties [17]. Moreover, single crystalline AgNPs with the minimization of low coordination defect sites show excellent stability and SERS properties. To further improve the SERS activity and stability of AgNPs and minimizing the use of precious Ag metal, immobilizing AgNPs with remarkable distribution and dispersion on various carbon materials (e.g., graphene oxide, graphene, carbon nanotubes and carbon nanofibers, etc.) are regarded as an effective strategy, due to the strong interactions between the AgNPs and carbon materials [18–20]. For example, Li et al. exploited modified graphene oxide as a support to synthesize reduced graphene oxide/AgNPs by chemical reduction method, and as-prepared composites were successfully applied to the SERS substrate, which gave high SERS activity toward Rhodamine 6G, accompanied by excellent stability [21].

Graphene oxide sheets (GOS), typical carbon materials, are prepared from the exfoliation of graphite oxide that basal planes mostly decorate with hydroxyl, epoxide, carbonyl and carboxyl groups [22]. Compared with other carbon materials, two-dimensional GOS has attracted tremendous attention as an ideal platform for growing and supporting metal nanoparticles due to its large surface area, low cytotoxicity, and good water solubility.

* Corresponding author.
E-mail address: xuzhiwei@tjpu.edu.cn (Z. Xu).
[1] These authors contributed equally to this work.

http://dx.doi.org/10.1016/j.apsusc.2017.01.159
0169-4332/

In particular, metal nanoparticles and metal cations can be directly attached on the GOS surface through physisorption, electrostatic binding or charge-transfer interactions [23–25].

Up to now, many methods have been conducted to synthetize GOS supported AgNPs (AgNPs/GOS) composites, such as thermal treatment, laser ablation, dry plasma synthesis and chemical reduction, etc. [3–8,23,26–29]. Compared with other approaches, the chemical route is uncomplicated and facile. Therefore, chemical reduction has emerged as a highly versatile strategy for synthesis of AgNPs/GOS composites. However, conventional chemical reduction routes to reduce precursors and prepare AgNPs/GOS composites from poisonous and hazardous reductants (sodium borohydride, formaldehyde and hydrazine), which may cause problems in the environment and health. Meanwhile, the sufficient reduction usually requires the excessive reductant, and thus the undesired oxidation product is inevitable [30,31]. Accordingly, efficient and uncontaminated irradiation reduction has been widely applied in fabricating AgNPs/GOS composites, such as γ-ray, microwave, ultraviolet and ultrasonic irradiation [30,32–36]. Of these techniques, γ-irradiation has been demonstrated to possess a number of advantages compared with other methods. For example, the high-energy γ-irradiation can uniformly generate reductant in the solution, which provides AgNPs in completely reduced, extremely pure, and very stable states during the reduction process. Moreover, γ-irradiation can significantly fragment AgNPs under high dosage (more than 100KGy), leading to small-sized AgNPs [31,37–41]. Therefore, γ-irradiation has exhibited tremendous potential in synthesis of AgNPs/GOS composites. Recently, Hareesh et al. used γ-irradiation induced reduction to facilely fabricate small-sized AgNPs decorated reduced graphene oxide composites in the presence of isopropyl alcohol and polyvinyl pyrrolidone [34]. Wang et al. found that 1-Ethyl-3-methylimidazolium acetate could act as scavenger and surfactant to prepare uniform and monodisperse AgNPs decorated reduced graphene oxide composites through γ-irradiation [33].

However, challenges remain in the γ-irradiation induced fabrication of AgNPs/GOS composites. Usually, to improve the dispersion and stabilization of nanoparticles, use of considerable surfactant or functional agent is inevitable. Accordingly, they have strongly absorb on the surface of nanoparticles, resulting in a discrepancy in the performance of composites [42–45]. Moreover, these strategies lack the crystalline structure and distribution control of AgNPs on GOS (i.e., they are always polycrystal structure with uniform or random distribution). On the other hand, GOS is directly used as precursor from exfoliation of graphite oxide by ultrasonic treatment, thereby decreasing the dimensions of GOS markedly [46]. Recently, to control the microcrystalline structures of AgNPs on the GOS without surfactant or functional agent, Hui et al. used ultrasonic irradiation for efficient control of crystalline structure, morphology and size of AgNPs by changing the concentration of Ag ions [30]. Gotoh et al. demonstrated that the preparation of metal nanoparticles decorated graphene sheets from cation exchange, the small-sized and homogeneously-dispersed noble metal nanoparticles could be obtained simultaneously to prevent the restacking of graphene sheets [47]. In addition, in our previous work, we reported that the graphite oxide interlayer distance was significantly increased by γ-irradiation treatment in the air [39]. Moreover, styrene functionalized graphene nanosheets were obtained efficiently by γ-irradiation, indicating that intercalation of graphite oxide is a facile method to achieve self-exfoliation and to prevent the agglomeration of functionalized graphene nanosheets during γ-irradiation [41]. Therefore, we combined the advantages of γ-irradiation technique and cation intercalation method to fabricate AgNPs/GOS composites, using imidazole silver nitrate ($Ag(im)_2NO_3$) as efficient intercalation complex into layers of graphite oxide, and subsequently inducing reduction and growth of interlamellar AgNPs via γ-irradiation. Composites were obtained at various concentrations of silver ions in order to explore the relations between the interplanar spacing of graphite oxide and the structures of the AgNPs. The possible mechanism of the evolution was proposed. In addition, the surface-enhanced Raman scattering (SERS) activity of these AgNPs/GOS composites was investigated.

2. Experimental details

2.1. Materials

Natural graphite flakes (200 mesh) were supplied by Qingdao AoKe ShiMo Co. Ltd., silver nitrate ($AgNO_3$), imidazole, and isopropanol alcohol (IPA) were supplied by Tianjin Kemiou Chemical Reagent Co., Ltd. Nitric acid (HNO_3, 68%), potassium permanganate, concentrated sulfuric acid (H_2SO_4, 98%) and phosphoric acid (H_3PO_4, 85%) were purchased from Tianjin chemical factory. All of reagents were at least of analytical reagent grade and used without further purification. All aqueous solutions were used with deionized water.

2.2. Preparation of AgNPs decorated GOS composites

Graphite oxide was synthesized from natural graphite flakes using a modified Hummers method, giving graphite oxide in a state of the pale yellow colloid [48,49]. The $Ag(im)_2NO_3$ was synthesized from previous reported procedure [50]. In briefly, the Ag complex was synthesized from 1.24 g $AgNO_3$ to 2.05 g imidazole, and the colorless crystals were obtained by slow evaporation of the solution at room temperature. The intercalation precursors have been prepared by magnetic stirring the mixture of 8 mM Ag aqueous solution and 50 ml graphite oxide suspensions for 24 h.

Simultaneously, 7.5 ml IPA and aqueous solution of $AgNO_3$ (0.1 M) with different volume of 2, 4, 8 and 12 ml were added to the mixture, followed by filled with water to the final volume of 100 ml for preparing solution, mixture allowed to stand 24 h. The weight ratios of components in the obtained mixture were presented in Table 1. And then, mixture has been purged by N_2 for 30 min. After sealed off, the mixture suspension was exposed under ^{60}Co γ-irradiation source with absorbed doses of 100 KGy (about 2.7 kGy/h dose rate) at room temperature. After irradiation, the produced AgNPs/GOS composite suspensions turned to be dark brown. After being isolated by centrifugation at the speed of 10,000 rpm for 6 min, the suspensions of the AgNPs/GOS composites were washed with deionized water thrice to remove residuary Ag^+, and freeze-dried with a condensing temperature of −40 °C at an inside pressure in less than 20 Pa. AgNPs/GOS powder was obtained. In a control experiment, we prepared GOS from exfoliation of graphite oxide by ultrasonic treatment, and used such GOS to replace graphite oxide as precursor, while other parameters remain unaltered.

Table 1
Concentration ratios of components in the obtained mixture.

sample name	$Ag(im)_2NO_3$: $AgNO_3$
$A_{0.5}$	1:0.5
A_1	1:1
A_2	1:2
A_3	1:3

2.3. Raman detection of crystal violet

10 μl aliquots of different concentrations of crystal violet (CV) in ethanol were dropped onto the as-prepared substrates (10 mm × 10 mm) and dried in a vacuum oven at 55 °C for SERS detection. The Raman spectra were recorded using a 532 nm laser with 1 mW power and a 50 × objective (1 μm^2 spot).

2.4. Characterization

Morphology and nanostructure of the prepared samples were observed using Hitachi H7650 transmission electron microscope (TEM) operated at an accelerating voltage of 100 kV. The high-resolution transmission electron microscopy (HRTEM) images were taken by a JEM-2100 model instrument operated at 300 kV. Samples for TEM and HRTEM were prepared by placing a drop of sample solution in ethanol onto a carbon-coated copper grid and dried in air. Noticeably, HRTEM images reflected from the central area of GOS. The distribution of AgNPs were studied by CSPM 5500 Atomic Force Microscope (AFM) and JEOL JSM-5900LV Energy Dispersive Spectrometer (EDS) equipped on Hitachi S-4800 field-emission scanning electron microscope (FE-SEM) at an accelerating voltage of 10 kV. The structural evolutions of composites were determined by Bruker D8 Discover X-ray Diffraction (XRD) using Cu Kα radiation (λ = 1.540 59 Å) with a scanning speed of 10°/min from 5 to 80°. The ultraviolet–visible (UV–vis) absorption spectra were measured on a Hitachi UV-3310 spectrophotometer within the wavelength region 200–600 nm. The chemical composition was analyzed by X-ray photoelectron spectroscopy (XPS, PHI 5700) with Al Kα excitation radiation. The Raman spectra were recorded on Renishaw in Via Raman Microscope with an excitation wavelength of 532 nm and a power of 1 mW.

3. Results and discussion

3.1. Morphology and microcrystalline structure of the AgNPs/GOS composites

XRD was employed to investigate the microcrystalline structure of composites. Fig. 1 showed XRD patterns of the graphite oxide, $Ag(im)_2NO_3$/graphite oxide, and AgNPs/GOS composites at different reaction concentrations of $AgNO_3$ ($A_{0.5}$–A_3). The pattern of graphite oxide exhibited the significant peak at 10.8°, which was assigned to the C(002) interplanar spacing (d_{002}) of 0.82 nm, $Ag(im)_2NO_3$/graphite oxide expanding to 0.88 nm because of sufficient intercalation of the silver complex [47]. After γ-irradiation, the prominent diffraction peaks of Ag(111), Ag(200), Ag(220) and Ag(311) crystallographic planes were observed clearly, revealing the formation of AgNPs in this composites [51]. In Fig. 1b, the AgNPs/GOS composites diffraction peaks of C(002) were nearly unchanged, while the intensity became barely discernible. The results illustrated the oxygen-containing functional groups still remained on the GOS and the GOS was successfully exfoliated during γ-irradiation [52,53]. In summary, AgNPs/GOS composites were successfully fabricated via this strategy.

The effect of the concentration of Ag ions on the structures of AgNPs/GOS composites was further investigated. The parameters calculated from XRD peaks and XPS spectra were summarized in Table 2. The d_{002} values were calculated by Bragg's law, the average particles size was estimated from Scherrere-Debye equation using

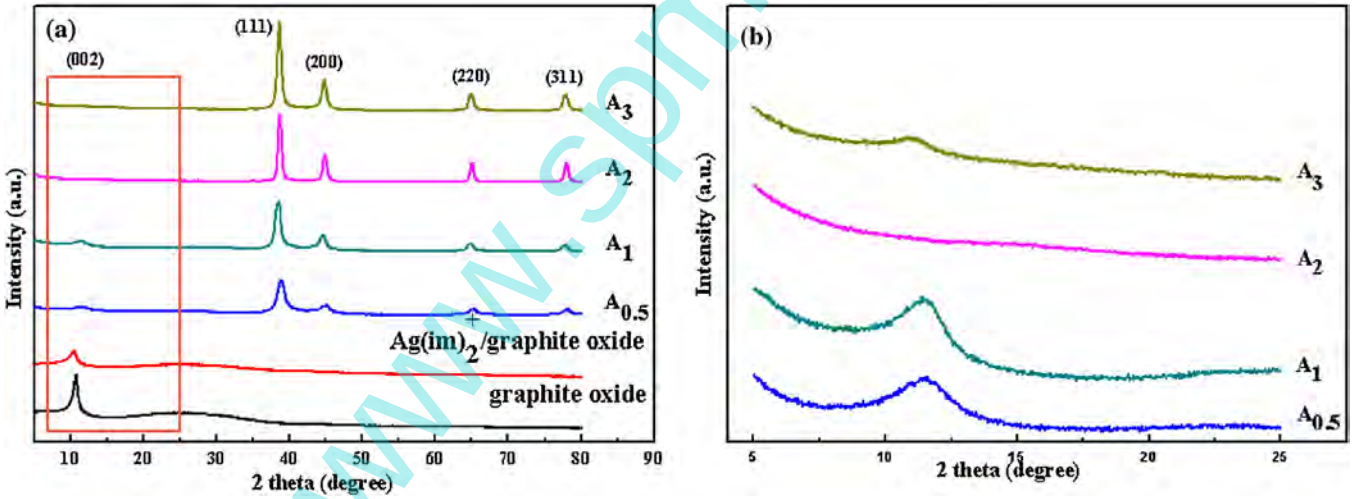

Fig. 1. X-ray diffraction patterns of graphite oxide, $Ag(im)_2NO_3$/graphite oxide and AgNPs/GOS composites ($A_{0.5}$–A_3): (a) full spectrum, (b) peaks of C(002) with fractionated gain.

Table 2
Parameters estimated from XRD peaks, HRTEM images and XPS spectra.

Sample name	XRD					TEM	XPS	
	Peaks of C (002)		Peaks of Ag (111)			Particle size (nm)	O/C[a]	Ag/C[a]
	2θ degree	d_{002} (nm)	FWHM (radian)	2θ degree	Particle size (nm)			
$A_{0.5}$	11.58	0.76	1.13	38.86	7.37	5.15	0.37	0.30
A_1	11.44	0.77	0.91	38.58	9.16	5.37	0.48	0.42
A_2	–	–	0.60	38.72	13.93	6.78	0.49	0.61
A_3	11.22	0.79	0.67	38.68	12.43	5.67	0.63	0.62

[a] The ratios of O/C and Ag/C were calculated from the equation as follows: A/B = A (wt.%)/B (wt.%), where A and B represent the corresponding elements; the weight content of element was obtained from XPS data.

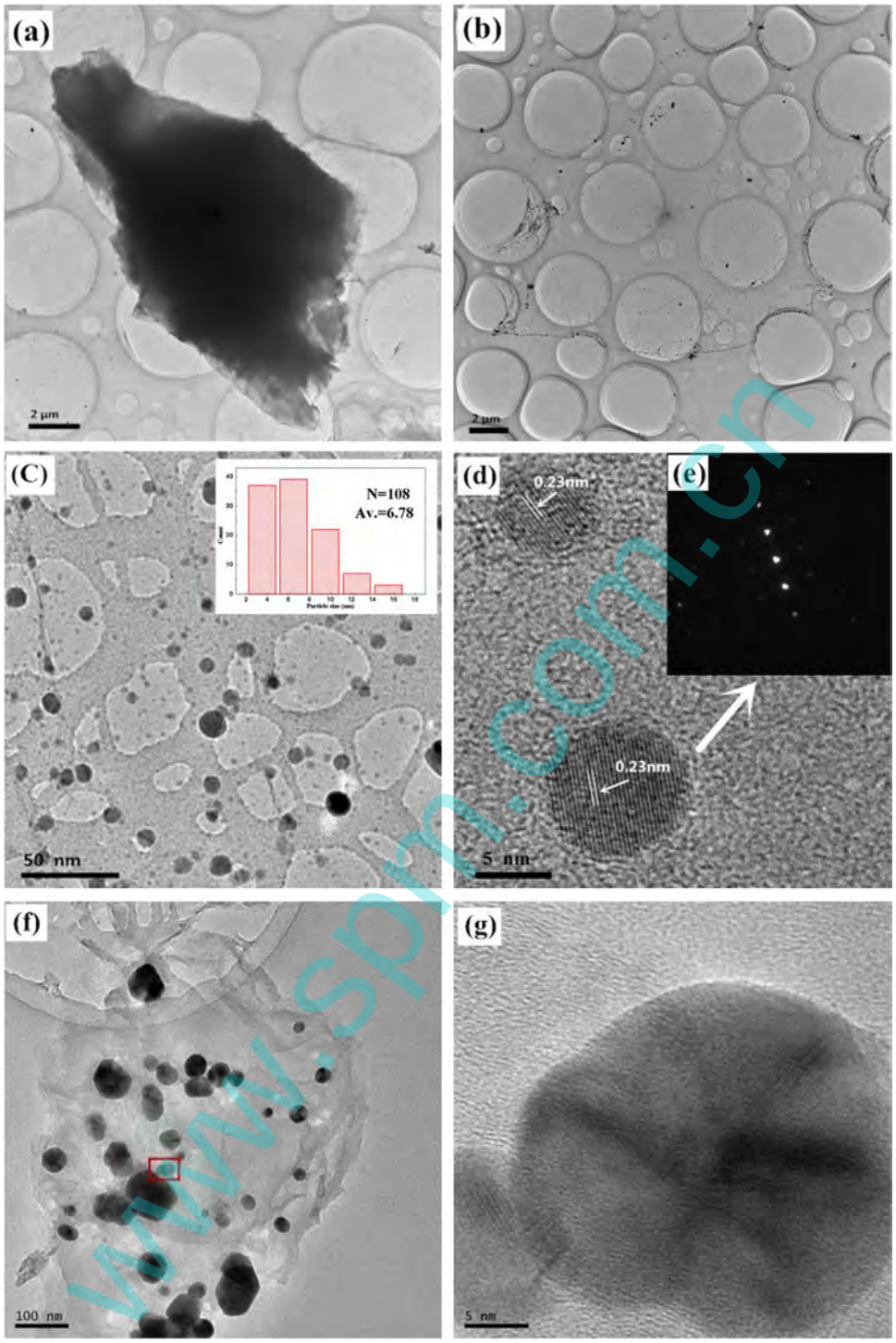

Fig. 2. TEM images of (a) $Ag(im)_2NO_3$/graphite oxide, (b) AgNPs/GOS composites of A_2, HRTEM images of (c) A_2 in central area of GOS, (d) high magnification image of A_2 and (e) corresponding SAED image, (f) control sample, which use GOS as precursor under the same conditions as A_2, (g) corresponding high magnification image.

the Ag(111) peak, because this peak had no interference from the diffraction peaks of carbon materials and thus could provide better accuracy [54]. The data directly showed that the size and content of AgNPs increased with increasing original concentration of Ag ions during the γ-irradiation, due to the significant improvement of crystal growth rates, which was consistent with previous research [55]. However, when the concentration of Ag ions increased to the level of A_3, the size of AgNPs was decreased. The extraordinary result illustrated that might exist other mechanism to influence the size of AgNPs. Therefore, we suspected the reason by following deduction. Obviously, the size of AgNPs were larger than d_{002} value of graphite oxide, and graphite oxide exhibited weak interactions between the interlayers [46]. Accordingly, growth of interlamellar AgNPs were limited by graphite oxide. In order to confirm such hypothesis, the d_{002} values of AgNPs/GOS composites were analyzed. Compared with original graphite oxide, the d_{002} of GOS in the AgNPs/GOS composites (A_3, A_1, $A_{0.5}$) decreased to 0.79, 0.77 and finally 0.76 nm at the 2θ angles of 11.22°, 11.44° and 11.58°, respectively. The d_{002} values decreased gradually as a result of the partial reduction of oxygen-containing functional groups on GOS with

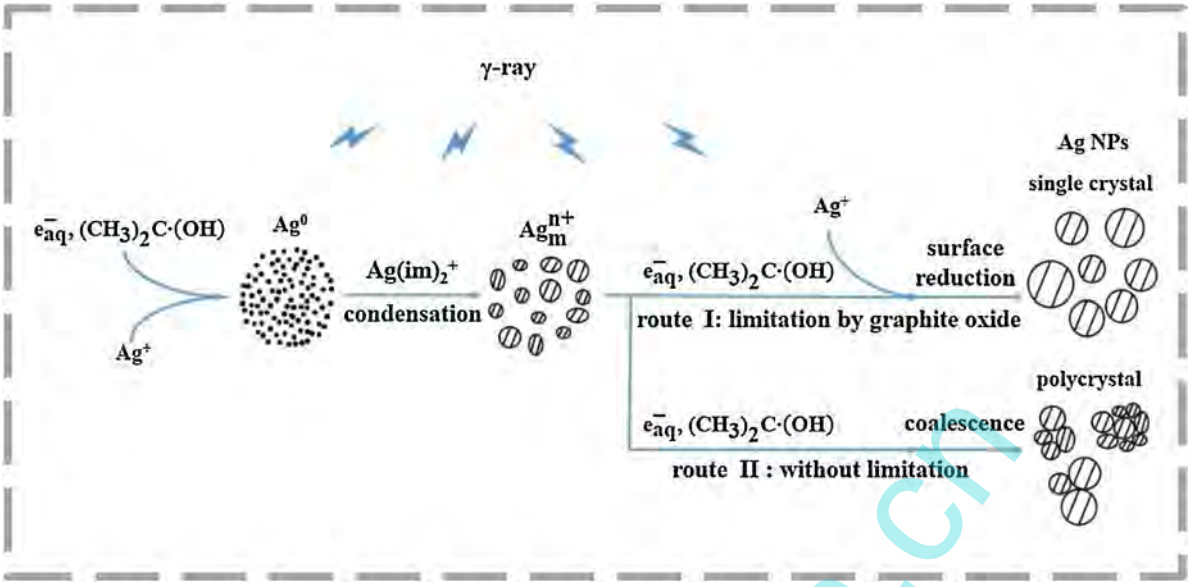

Fig. 3. Illustration of two growth routes of AgNPs on graphite oxide (I) and GOS (II), respectively.

varying degrees [56]. The reduction degree of oxygen-containing functional groups was described via ratios of O/C in Table 2. Particularly, the disappearance of GOS characteristic peak of A_2 illustrated that GOS was exfoliated completely [57]. Such similar changing trend of d_{002} values and AgNPs size provided powerful evidence to support the view that interlamellar space of graphite oxide limited particles growth, because larger layer spacing exhibited weaker limitation, resulting in large AgNPs size. Therefore, the sample of A_2 had the largest Ag size because limitation disappeared after GOS completely exfoliated. Herein, we suggested that the interlamellar spacing played a key role in limiting size of particles. However, it was unclear that why GOS of A_3 restacked during irradiation. The possible reason was that the excessive Ag^+ reduced repulsion between the layers because GOS was electronegative colloid, which led to exfoliation degree of GOS decreased.

The morphology and structure features of composites were investigated by TEM and HRTEM. It was clearly seen in Fig. 2a that the $Ag(im)_2NO_3$/graphite oxide agglomerated to a greater extent with above ten micrometers lateral size. After irradiation for $Ag(im)_2NO_3$/graphite oxide in Fig. 2b, we could find that the substrate of graphite oxide was exfoliated to GOS with the same sheets size and AgNPs were too small to be observed clearly. The morphology of AgNPs/GOS composites in the central (Fig. 2c) and edge area (Fig. S1) of GOS revealed that AgNPs with monodispersity were successfully attached on the GOS surface. The crystalline structure of AgNPs/GOS composites were further confirmed by HRTEM and the SAED pattern (Fig. 2d and inset). The fringe lattice of AgNPs was found to be 0.23 nm, which corresponded to the Ag(111) lattice spacing (0.236 nm). The well-resolved lattice fringes and regularly dotted pattern indicated that the AgNPs had a single crystalline structure [30,54]. In a control experiment, GOS were directly used as precursor by ultrasonic treatment. The products consisted of irregularly distributed and larger-sized nanoparticles with obvious aggregation, and almost no single crystalline AgNPs were found on the GOS surface (Fig. 2f). Moreover, the diameter of GOS decreased to hundreds of nanometers due to strong cavitation of sonication [46]. However, the size of AgNPs was still within nanoscale, indicating that the size of AgNPs could be fragment by γ-irradiation in the high dose rate. Thus, it was confirmed that based on synergism of interlamellar limitation of graphite oxide and fragmentation ability of γ-irradiation, the growth of interlamellar AgNPs could be prevented from aggregating.

The growth of AgNPs was explained by the following mechanism, which was also schematically depicted in Fig. 3. The radiolysis of aqueous solvent system, the formation of hydrated electrons (e^-_{aq}), hydroxyl radicals (·OH) and hydrogen radicals (•H) were the first step in the radiolytic growth of AgNPs. The chemical yields for e^-_{aq}, and •OH were reported to be 2.7, 0.6 and 2.8, respectively. Thus, 2-propanol was used as a scavenger to convert •OH and •H to 2-propanol radicals ($(CH_3)_2C\cdot OH$) [58]:

$$H_2O \xrightarrow{\gamma\text{irradiation}} {}^{\bullet}H + {}^{\bullet}OH + e^-_{aq} + H_2O_2 + H^+ \quad (1)$$

$$^{\bullet}H\,(^{\bullet}OH) + (CH_3)_2CHOH \rightarrow H_2\,(H_2O) + (CH_3)_2C^{\bullet}\,(OH) \quad (2)$$

Since the electrochemical potential of the Ag^+/Ag^0 was more positive than that of the Ag complex system, The interlamellar Ag^+ was reduced by the e^-_{aq} and $(CH_3)_2C\cdot OH$:

$$Ag^+ + e^-_{aq} \rightarrow Ag^0 \quad (3)$$

$$Ag^+ + (CH_3)_2C\cdot(OH) \rightarrow Ag^0 + (CH_3)_2CO + H^+ \quad (4)$$

However, individual atom was unstable in aqueous solution owing to high surface energy, and Ag complex ions had higher stability than Ag ions. The oligomeric clusters were formed from combining silver atoms and complex ions via condensation reactions, meanwhile directly immobilized at oxygen-containing functional groups, and the nature of certain intermediate clusters had been elucidated by analogy with previous report such as $Ag_2(im)_2^+$, $Ag_4(im)_4^{2+}$, $Ag_9(im)_2^+$, etc. [37,55]. Therefore, as the nuclei, positively charged clusters were well dispersed on the electronegative surface of GOS with excellent stability via charge-transfer interactions. Meanwhile the clusters could more or less be neutralized, which favored their condensation to form larger ones, and we simply designated the small clusters as Ag_m^{n+}. According to Eqs. (5) and (6), under the interlamellar limitation of graphite oxide, the growth of Ag_m^{n+} was protected from further reaction with each other, and the Ag ions were reduced in situ by the radicals and hydrated electrons on clusters surface. When amount of *m* exceeded threshold, the electrochemical potential of Ag_m^{n+} was higher than Ag ions. Meanwhile concentration of Ag ions was too low to emerge slow reaction rate, the positively charged clusters were reduced [37,59], resulting in formation of small-sized and single crystalline AgNPs. In a control experiment, positively charged clusters were generated on GOS. However, the growth of clusters

was ineffectively protected from further coalescent reaction without limitation. Thereby, AgNPs agglomerated to larger and larger structures according to Eq. (7).

$$Ag_m^{n+} + iAg^+ + ie_{aq}^- \,(\text{or } i(CH_3)_2C\cdot(OH)) \rightarrow Ag_{m+i}^{n+} + \left(i(CH_3)_2CO + iH^+\right) \quad (5)$$

$$Ag_{m+i}^{n+} + ne_{aq}^- \,(\text{or } n(CH_3)_2C\cdot(OH)) \rightarrow Ag_{m+i} + (n(CH_3)_2CO + nH^+) \quad (6)$$

$$Ag_{m1}^{n1+} + Ag_{m2}^{n2+} \rightarrow Ag_{m1+m2}^{(n1+n2)+} \quad (7)$$

The effect of the Ag ions concentration on the size of AgNPs/GOS composites was further investigated. Fig. 4a–c shows the typical HRTEM images of AgNPs/GOS composites at different concentrations and the corresponding size of AgNPs was reported in Table 2. The data had shown that the size of AgNPs calculated from XRD was larger than TEM, while the changing trend of the AgNPs size from two characterizations were accordant. In other word, the particle size increased with increasing Ag ions concentration, and abnormally, sample A_2 had the largest size. It directly evidenced that the particles size in center was smaller than the whole area, because TEM images picked from central area of GOS. Such inconsistent results of AgNPs size from two characterizations were another indication of interlamellar limitation. Similarly to the exfoliation process of graphite [53], it could be explained that the graphite oxide was exfoliated to GOS from the edge to the central area of the graphite oxide. the limitation degree of particles growth in central area was stronger than other area. Thereby, the particles in center exhibited the minimum size. In order to describe the distribution of AgNPs accurately, EDS and AFM had been used.

EDS linear scanning was applied to analyze elemental distribution in the AgNPs/GOS composites. As shown in Fig. 5a, the outline of the AgNPs/GOS composites were obvious, the content of carbon element did not change significantly, while the content of silver element decreased firstly and then increased gradually along the white line from top to bottom of the AgNPs/GOS composites surface (Fig. 5b). Similarly, AFM analysis (Fig. 5c, d) showed that the height of composites decreased gradually from the side to the middle, it provided strong evidence that the size of AgNPs exhibited parabolic distribution on the surface of GOS, since thickness of sheet changed non-significantly under the same GOS. In summary, the AgNPs attached on the GOS with parabolic distribution as a result of the interlamellar limitation of graphite oxide.

The comparison of our samples with other AgNPs/GOS composites in method of preparation and structures was listed in Table 3, which revealed obvious advantages of our work. Namely, we obtained GOS supported AgNPs with single crystalline structure and parabolic distribution without surfactant and functional agent.

3.2. Component and interfacial bonding of AgNPs/GOS composites

To investigate the chemical state of graphite oxide and the AgNPs/GOS composites, the XPS spectra were examined. In Fig. 6a, the survey spectra clearly indicated the existence of C, O in graphite oxide and the existence of C, O, Ag in the composites. As shown in Fig. 6b, the Ag 3d XPS spectra showed strong signals at 368.78 and 374.78 eV, which corresponded to Ag $3d_{5/2}$ and Ag $3d_{3/2}$ binding energies, respectively, and no characteristic peak of Ag_2O (367.8 eV) or AgO (367.4 eV) was observed as well. The positions of these peaks proved that silver was present only in metallic form, suggesting that the pure AgNPs were anchored on the GOS surface [23]. The C 1s spectrum of graphite oxide (Fig. 6c) could be deconvoluted into three components with binding energy at 284.8, 286.9 and 288.0 eV, which were ascribed to C—C (unoxidized graphite carbon skeleton), C—O (hydroxyl and epoxide) and C═O (carboxyl) groups,

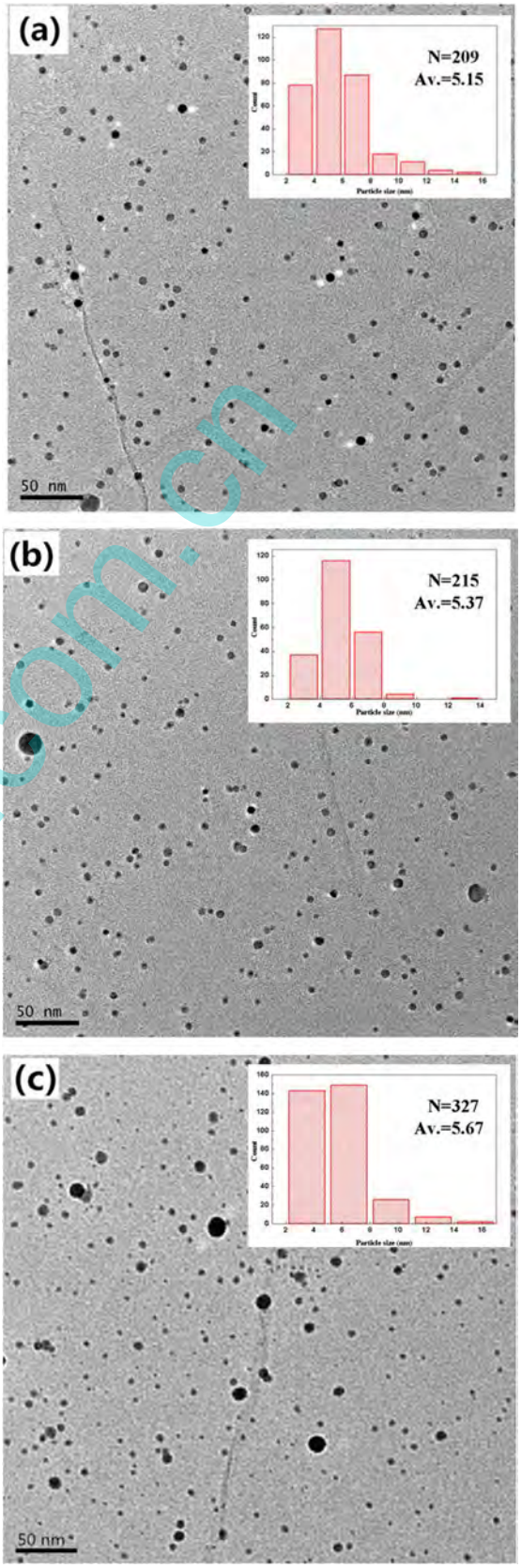

Fig. 4. HRTEM images of the different AgNPs/GOS composites in central area of GOS: (a) $A_{0.5}$ (b) A_1 (c) A_3.

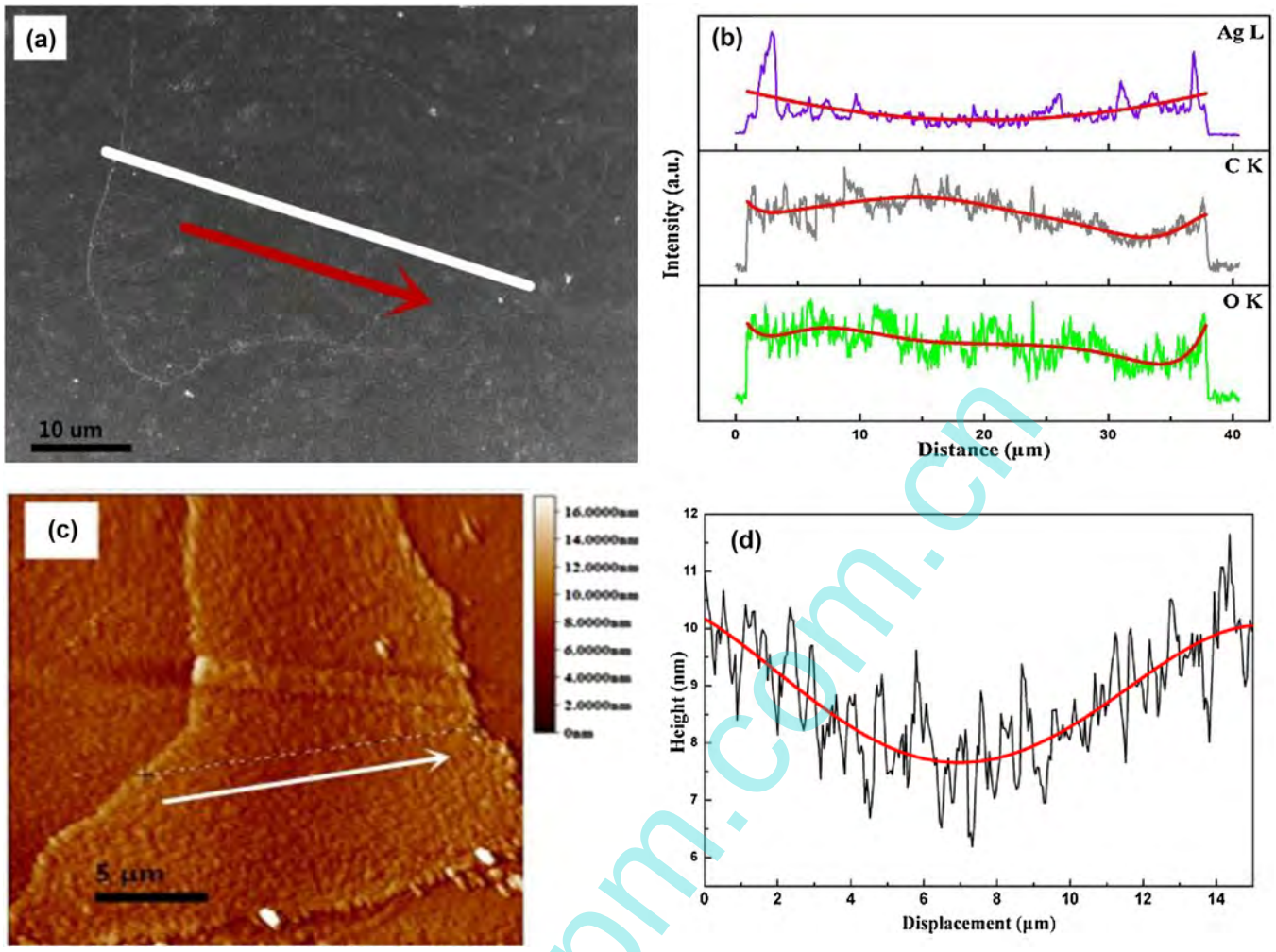

Fig. 5. AgNPs/GOS composites of sample A_2: (a) SEM image (the dotted line indicates outline of composites), (b) distribution of silver, carbon and oxygen elements along the white line (measured by EDS linear scanning system), (c) image of AFM tapping mode, (d) height distribution along the dotted line.

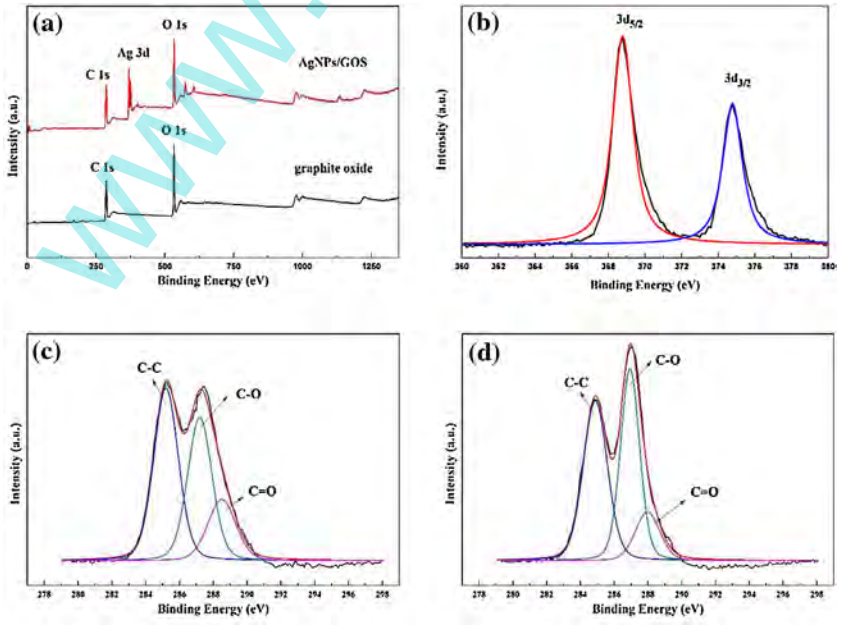

Fig. 6. XPS survey scans of (a) graphite oxide and AgNPs/GOS of A_2, (b) Ag 3d XPS spectra of AgNPs/GOS, (c) C 1 s XPS spectra of AgNPs/GOS and graphite oxide (d).

Table 3
Structure and preparation method of AgNPs/GOS composites.

Sample	Reduction method	Surfactant or functional agent	Dispersion	Distribution	Crystalline structure	Ref.
GOS/AgNPs	chemical reduction by sodium borohydride	trisodium citrate[b]	monodispersion	random and wide	polycrystal	[6]
GOS/AgNPs	chemical reduction by $NaBH_4$ in toluene solution	cetyl trimethyl ammonium bromide[b]	partial aggregation	random	polycrystal	[4]
Ag@GOS	chemical reduction by glucose in Supercritical carbon dioxide	Supercritical carbon dioxide[b]	partial aggregation	random	polycrystal	[28]
Ag-GOS	chemical reduction through mirror reaction	MnOOH[c,d]	aggregation	random and narrow	polycrystal	[5]
Ag-thiolated GOS	chemical reduction by $NaBH_4$	NaSH[c]	monodispersion	uniform	polycrystal	[7]
GOS–chitosan-Ag	chemical reduction by $NaBH_4$	chitosan[c]	aggregation	wide	polycrystal	[8]
Ag/GOS	Dopamine inducing the spontaneous formation	dopamine[c]	monodispersion	random and narrow	–	[3]
AgNPs/GOS	chemical reduction by sodium citrate	–	aggregation	wide	–	[29]
GOS-Ag	chemical reduction by glucose	–	aggregation	uniform	polycrystal	[23]
AgNPs/GOS	Laser Ablation	–	aggregation	wide	polycrystal	[26]
GOS-Ag	Dry plasma synthesis	–	excellent dispersion	uniform and narrow	polycrystal	[27]
Ag-GOS	photochemical reduction by UV irradiation in ethanol	–	monodispersion	uniform	polycrystal	[36]
Ag/rGO[a]	L-arginine assisted reduction by Microwave	L-arginine[b]	monodispersion	uniform and narrow	polycrystal	[35]
AgNPs–rGO	heat-assisted reduction by ultrasonication	–	excellent dispersion	narrow	polycrystal	[32]
AgNP–GOS	vitamin C-assisted reduction by ultrasonication	–	partial aggregation	random and wide	singe crystal	[30]
Ag-rGO	gamma irradiation induce reduction in the presence of IPA	polyvinyl pyrrolidone[b]	excellent dispersion	random and wide	polycrystal	[34]
Ag-rGO	Ionic-liquid-assisted reduction by gamma irradiation	1-Ethyl−3-methylimidazolium acetate[b]	monodispersion	uniform	–	[33]
Ag NPs/GOS	gamma irradiation induce reduction in the presence of IPA	–	monodispersion	parabolic	singe crystal	This work

[a] reduced graphene oxide sheets.
[b] stabilizing or controlling structure of AgNPs by surfactant.
[c] stabilizing or controlling structure of AgNPs by functionalization.
[d] manganese oxyhydroxide.

respectively [33]. The C 1s XPS spectrum of AgNPs/GOS composites was also deconvoluted into three peaks at 285.1, 287.1, 288.4 eV assigned to C—C, C—O and C═O, respectively (Fig. 6d). These results indicated that a large number of oxygen-containing functional groups on the surface of GOS still retained after γ-irradiation. In addition, the intensity of the band at 287.1 eV (C—O) was decreased which indicated the partial reduction of graphite oxide to GOS.

UV–vis spectra was used to record the change of graphite oxide to AgNPs/GOS composites. In Fig. 7a, the two characteristic peaks of graphite oxide were a signal at 233 nm, which described the $\pi \rightarrow \pi^*$ transitions of the aromatic C—C bonds and a shoulder at 300 nm, which was related to the $n \rightarrow \pi^*$ transitions of the C═O bonds [60]. As shown in the UV–vis spectra of AgNPs/GOS composites (Fig. 7b), the formation of AgNPs was indicated by the surface plasmon resonance peak of AgNPs at 412 nm in the AgNPs/GOS composites, which was similar to previous studies [23,67]. Moreover, it was reported that AgNPs appeared spherical shape when its sharp peak was in the range of 400–500 nm [6], which was consistent with the TEM result. To further confirm the interactions between graphite oxide and AgNPs, the FI-IR spectra of the samples were examined. Fig. 7c showed the shape of graphite oxide and AgNPs/GOS composites were similar. As for AgNPs/GOS, the intensity of the C═O stretching vibration decreased, whereas the C═C stretching vibration increased. This change proved the interactions between the AgNPs and the oxygen-containing functional groups of the GOS by forming a chemical bond or electrostatic attraction, which was consistent with a similar previous report [30,61].

3.3. Surface-enhanced Raman Scattering properties

Raman spectra of all samples was shown in Fig. 8a. Two characteristic D and G peaks were observed. The D band (~1346 cm^{-1}) originating from the breathing mode of κ-point and the G band (~1591 cm^{-1}) provided the information of the tangential stretching mode of E_{2g} phonon [54]. It was clearly noticed that intensities of two peaks were enhanced after decoration of AgNPs on the surface of GOS. Moreover, compared with other AgNPs/GOS composites, A_2 exhibited larger size (13.9 nm) and excellent Ag content (the Ag/C of A_2 was only 0.01 less than that of A_3), as well as complete exfoliation of GOS. The electromagnetic enhancement, dominant factor for SERS enhancement, could benefit largely from these structure features [17,62]. Therefore, sample of A_2 exhibited the best SERS properties (6.3 fold than pristine graphite oxide).

CV, one of the widely used standard SERS probe, it is chosen to probe the SERS activity with the AgNPs/GOS composites. The SERS spectra of CV absorbed on optimal AgNPs/GOS composites substrates with different concentrations were excited. As shown in Fig. 8c, strong Raman signals were monitored on the AgNPs/GOS composites substrates at 10^{-4} M concentration of CV. The peaks at 805, 914, 1176, 1373, 1619 cm^{-1} were agreement with pure CV and previous report [68]. As the concentration of CV decreased, the

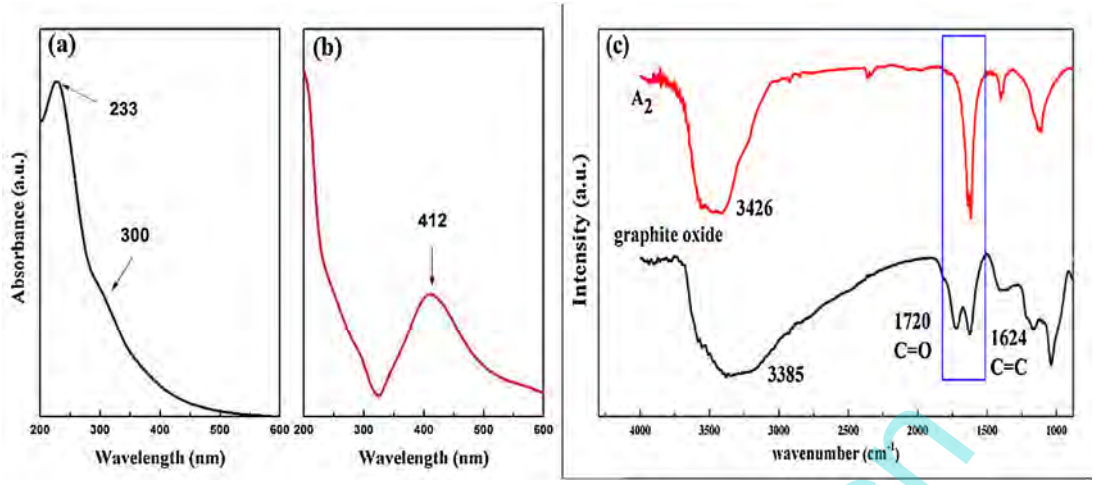

Fig. 7. UV–vis absorption spectra of graphite oxide (a) and AgNPs/GOS composites of A_2 (b). FI-IR absorption spectra of graphite oxide and composites of A_2 (c).

Table 4
SERS properties of various graphene oxide-based Ag nanostructures.

SERS substrate	Reduction method	sample preparation for SERS	excitation parameters		Dyes	detection limit (M)	EF	Ref.
			Wavel-ength (nm)	Power (mW)				
GOS-Ag	chemical reduction by sodium citrate	drop-cast onto the si substrate	633	2	CV	10^{-6}	–	[10]
			633	2	R6G	10^{-6}		
			633	2	MG	10^{-6}		
			633	2	MB	10^{-6}		
GOS- Ag	photochemical reduction	drop-cast onto the si substrate	514	2	R6G	8×10^{-6}		[11]
GOS/CS/AgNPs	chemical reduction by sodium citrate	disperse in organic solvents	514	–	MB	10^{-7}	–	[12]
GOS/Ag	–	spin-coate on the si substrate	532	–	R6G	10^{-7}	4.1	[64]
Ag–GOS	chemical reduction by tryptophan	disperse in aqueous solutions	532	35	CV	10^{-10}	1.6×10^5	[13]
AgNP@GOS	chemical reduction by 1,5-pentanediol	drop-cast onto APTES-modified Si substrates	532	0.17	R6G	10^{-10}	4.8×10^5	[65]
	0.17		532	0.17	CV	10^{-9}	4.8×10^5	
AgNPs/GOS	gamma irradiation induced reduction in the presence of IPA	drop-cast onto the si substrate	532	1	CV	10^{-7}	1.3×10^6	This work
GOS/Ag/TiO_2	chemical reduction by $NaBH_4$	disperse in aqueous solutions	785	–	MB	10^{-9}	2.1×10^7	[66]
Au@AgNPs/GOS	chemical reduction by trisodium citrate	cast onto the APTES-modified Si substrates	532	–	R6G	10^{-9}	7×10^7	[63]

peak intensity of CV became weakened. At 10^{-8} M, Raman signal of CV on the substrate was disappeared. Thereby, the detection limit of CV was estimated to be around 10^{-7} M. However, the strong GOS bands might become a huge disturbance in the SERS signals of molecules at low concentrations [14,18]. To improve the rigor of the optimization experiment with different composites, the SERS CV signals were recorded on the different AgNPs/GOS composites. Fig. S2 indicated that the sample of A_2 prepared SERS substrates exhibited the best SERS properties, consistent with the above conclusion. In summary, under our SERS substrates, the detection limit of CV was estimated to be around 10^{-7} M. In addition, the average enhancement factor (*EF*) calculated according to the following Formula (8):

$$EF = I_{SERS}N_{bulk}/I_{bulk}N_{surface} \quad (8)$$

Where I_{SERS} and I_{bulk} are the peak intensities of 10^{-7} M CV on the AgNPs/GOS composites substrates and 0.01 M CV on a silicon substrate at 1176 cm^{-1}, respectively. I_{SERS} and I_{bulk} were directly obtained from the SERS spectra, 9426.1 and 715.2, respectively. $N_{surface}$ and N_{bulk} are the number of CV molecules excited by the laser beam on the AgNPs/GOS composites and silicon substrate, respectively. These data calculated form the concentration of surface or bulk sample and the corresponding area of sample (AS) [13,63]. The surface area of the substrate is 10 mm × 10 mm. The $N_{surface}$ and N_{bulk} were assumed to be 10^{-7} mol $L^{-1} \times 10\,\mu l \times N_A \times AS/100\,mm^2$ and 10^{-2} mol $L^{-1} \times 10\,\mu l \times N_A \times AS/100\,mm^2$, respectively. Accordingly, the *EF* of the AgNPs/GOS composites was about 1.3×10^6. The results of the experiment confirmed that the composites exhibited excellent SERS properties, which were reflected in the comparison of our samples with previous AgNPs/GOS composites from Table 4. It clearly showed that our AgNPs/GOS composites exhibited high *EF*, but a relatively low detection limit compared with other AgNPs/GOS composites. This abnormal phenomenon could be explained through following discussion. Obviously, The *EF* mainly depended on two sources: the electromagnetic mechanism (a factor of 10^6–10^8 enhancement) and the chemical mechanism (a factor of 10–100 enhancement) [14], when enough AgNPs attached

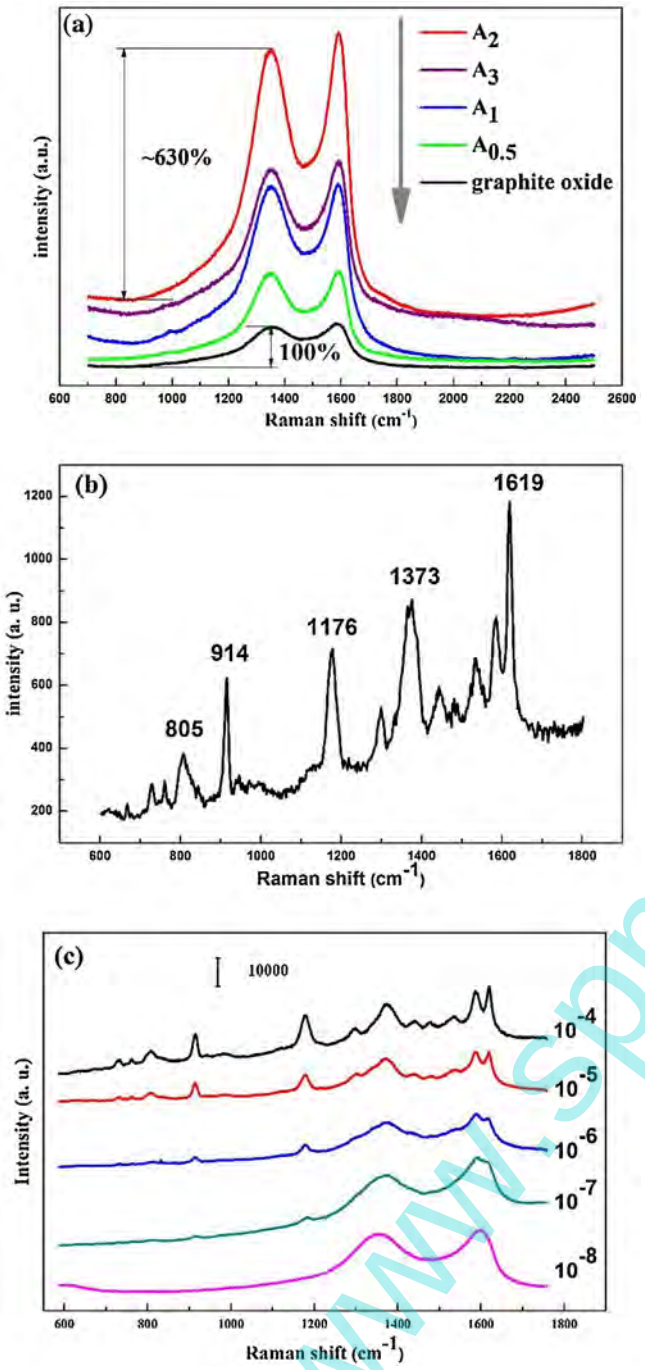

Fig. 8. (a) Raman spectra of graphite oxide and different AgNPs/GOS composites ($A_{0.5}$–A_3), SERS spectra of (b) CV with 10^{-2} M on the silicon substrate and (c) different concentrations of CV (10^{-4}–10^{-8}) absorbed on the optimal AgNPs/GOS composites substrate.

on the surface of material, electromagnetic enhancement became the dominant factor due to the resonances occurring on the metal surface [17]. Consequently, the AgNPs/GOS composites exhibited high *EF* value for their excellent structure of AgNPs. However, the enhancement effect was only one reason for detection limit. The suppressing effect of the macrocyclic probe molecules on the AgNPs/GOS composites could not be ignored, due to the charge transfer interaction between probe molecules and graphene oxide. And thus, the primary reason of low detection limit was the huge disturbing effect of the strong D/G bands of GOS. Secondly, as we know, the detection limit also depended on the experimental parameters. For example, diverse excitation power and wavelengths lead to different detecting depths, resulting in influence on the detection limit. Although AgNPs/GOS composites in this work could not compare the SERS performance objectively, due to not all literatures provided detection limit and *EF* in the same condition, it was enough to directly observe a trace amount of organic dyes.

On the other hand, the SERS experiment about the reproducibility of AgNPs/GOS composites was further achieved. The SERS signals of CV recorded on the optimized AgNPs/GOS composites which were stored in the dark for 13 days reached 95.3% of its original value (Fig. S3a), and it was more than the value 87.6% for the control sample (Fig. S3c), indicating that the single crystalline AgNPs was benefit for SERS stability.

4. Conclusions

In this work, GOS supported AgNPs with single crystalline structure and parabolic distribution had been obtained without surfactant or functional agent, $Ag(im)_2NO_3$ was used as efficient intercalation precursor into the layers of graphite oxide, and subsequently the reduction and growth of interlamellar AgNPs were induced via γ-irradiation. The parameters calculated from XRD peaks showed that size of AgNPs increased with d_{002} values increasing, which provided strong evidence to support the opinion that the interlamellar spacing of graphite oxide limited AgNPs growth. Based on the synergism of fragmentation ability of γ-irradiation and interlamellar limitation of graphite oxide, minor sized (below 13.9 nm) and single crystalline AgNPs were obtained. More importantly, owing to the exfoliation of GOS from the edge to the central area of graphite oxide, the size and content of AgNPs had exhibited parabolic distribution on GOS, which could be demonstrated by AFM and EDS images. In addition, complete exfoliation degree of GOS and large-sized AgNPs were obtained simultaneously under appropriate reaction condition. On the other hand, Raman spectra showed that the Raman signals of optimal composites were dramatically enhanced (6.3 fold than pristine graphite oxide) due to generating plenty hot spots on their surface. Such composites exhibited outstanding SERS properties for crystal violet with the enhancement factor of 1.3×10^6 and the detection limit of approximately 1.0×10^{-7} M, illustrating that the AgNPs/GOS composites could be applied to trace detection of organic dyes molecules. This study indicated that the interlamellar limitation of graphite oxide could protect growth of AgNPs, which provided a guide to efficiently synthesize single crystalline metal nanoparticles with parabolic distribution decorated GOS composites based on γ-irradiation technique.

Acknowledgments

The work was funded by the National Natural Science Foundation of China (11575126), the Natural Science Foundation of Tianjin (16JCZDJC37800, 16JCYBJC17700) and the Science and Technology Plans of Tianjin (16ZXCLGX00090, 15PTSYJC00230).

Appendix A. Supplementary data

Supplementary data associated with this article can be found, in the online version, at http://dx.doi.org/10.1016/j.apsusc.2017.01.159.

References

[1] T.K. Sau, A.L. Rogach, F. Jackel, T.A. Klar, J. Feldmann, Properties and applications of colloidal nonspherical noble metal nanoparticles, Adv. Mater. 22 (2010) 1805–1825.

[2] T.K. Sau, A.L. Rogach, Nonspherical noble metal nanoparticles: colloid-chemical synthesis and morphology control, Adv. Mater. 22 (2010) 1781–1804.
[3] E.K. Jeon, E. Seo, E. Lee, W. Lee, M.K. Um, B.S. Kim, Mussel-inspired green synthesis of silver nanoparticles on graphene oxide nanosheets for enhanced catalytic applications, Chem. Commun. 49 (2013) 3392–3394.
[4] A.Q. Mao, D.H. Zhang, X. Jin, X.L. Gu, X.Q. Wei, G.J. Yang, X.H. Liu, Synthesis of graphene oxide sheets decorated by silver nanoparticles in organic phase and their catalytic activity, J. Phys. Chem. Solids 73 (2012) 982–986.
[5] W.S. Bai, F. Nie, J.B. Zheng, Q.L. Sheng, Novel silver nanoparticle-manganese oxyhydroxide-graphene oxide nanocomposite prepared by modified silver mirror reaction and its application for electrochemical sensing, ACS Appl. Mater. Interfaces 6 (2014) 5439–5449.
[6] M.R. Das, R.K. Sarma, S. Borah, R. Kumari, R. Saikia, A.B. Deshmukh, M.V. Shelke, P. Sengupta, S. Szunerits, R. Boukherroub, The synthesis of citrate-modified silver nanoparticles in an aqueous suspension of graphene oxide nanosheets and their antibacterial activity, Colloids Surf. B 105 (2013) 128–136.
[7] J.D. Kim, T. Palani, M.R. Kumar, S. Lee, H.C. Choi, Preparation of reusable Ag-decorated graphene oxide catalysts for decarboxylative cycloaddition, J. Mater. Chem. 22 (2012) 20665.
[8] R. Rajesh, E. Sujanthi, S.S. Kumar, R. Venkatesan, Designing versatile heterogeneous catalysts based on Ag and Au nanoparticles decorated onchitosan functionalized graphene oxide, Phys. Chem. Chem. Phys.: PCCP 17 (2015) 11329–11340.
[9] T. Georgakopoulos, M.V. Sofianou, K. Pomoni, N. Todorova, T. Giannakopoulou, C. Trapalis, The environment effect on the electrical conductivity and photoconductivity of anatase TiO_2 nanoplates with silver nanoparticles photodeposited on {101} crystal facets, Mater. Sci. Semicond. Process. 56 (2016) 386–393.
[10] G.H. Ding, S. Xie, Y. Liu, L. Wang, F.G. Xu, Graphene oxide-silver nanocomposite as SERS substrate for dye detection: effects of silver loading amount and composite dosage, Appl. Surf. Sci. 345 (2015) 310–318.
[11] J.L. Chen, X.L. Zheng, H. Wang, W.T. Zheng, Graphene oxide-Ag nanocomposite: in situ photochemical synthesis and application as a surface-enhanced Raman scattering substrate, Thin Solid Films 520 (2011) 179–185.
[12] M.M. Wan, Z.M. Liu, S.X. Li, B.W. Yang, W. Zhang, X.C. Qin, Z.Y. Guo, Silver nanoaggregates on chitosan functionalized graphene oxide for high-performance surface-enhanced Raman scattering, Appl. Spectrosc. 67 (2013) 761–766.
[13] B.W. Yang, Z.M. Liu, Z.Y. Guo, W. Zhang, M.M. Wan, X.C. Qin, H.Q. Zhong, In situ green synthesis of silver–graphene oxide nanocomposites by using tryptophan as a reducing and stabilizing agent and their application in SERS, Appl. Surf. Sci. 316 (2014) 22–27.
[14] S. Sun, P. Wu, Competitive surface-enhanced Raman scattering effects in noble metal nanoparticle-decorated graphene sheets, Phys. Chem. Chem. Phys. 13 (2011) 21116–21120.
[15] J. Sun, X.Y. Teng, J.X. Yang, One pot synthesis of a highly water-dispersible hybrid glucose carbides and reduced graphene oxide material with superior electrical capacitance, J. Mater. Sci. 48 (2013) 8277–8286.
[16] A.S. Voronin, F.S. Ivanchenko, M.M. Simunin, High performance hybrid rGO/Ag quasi-periodic mesh transparent electrodes for flexible electrochromic devices, Appl. Surf. Sci. 364 (2016) 931–937.
[17] Q.L. Huang, J.M. Wang, W.X. Wei, Q.X. Yan, C.L. Wu, X.S. Zhu, A facile and green method for synthesis of reduced graphene oxide/Ag hybrids as efficient surface enhanced Raman scattering platforms, J. Hazard. Mater. 283 (2015) 123–130, 8.
[18] W. Ren, Y.X. Fang, E.K. Wang, A binary functional substrate for enrichment and ultrasensitive SERS spectroscopic detection of folic acid using graphene oxide/Ag nanoparticle hybrids, ACS Nano 5 (2011) 6425–6433.
[19] J. Lee, K. Lee, S.S. Park, Environmentally friendly preparation of nanoparticle-decorated carbon nanotube or graphene hybrid structures and their potential applications, J. Mater. Sci. 51 (2015) 2761–2770.
[20] X. Chen, S.J. Chen, J.Y. Wang, Screening of catalytic oxygen reduction reaction activity of metal-doped graphene by density functional theory, Appl. Surf. Sci. 379 (2016) 291–295.
[21] S.K. Li, Y.X. Yan, J.L. Wang, S.H. Yu, Bio-inspired in situ growth of monolayer silver nanoparticles on graphene oxide paper as multifunctional substrate, Nanoscale 5 (2013) 12616–12623.
[22] S. Stankovich, D.A. Dikin, G.H. Dommett, K.M. Kohlhaas, E.J. Zimney, E.A. Stach, R.D. Piner, S.T. Nguyen, R.S. Ruoff, Graphene-based composite materials, Nature 442 (2006) 282–286.
[23] W. Shao, X.F. Liu, H.H. Min, G.H. Dong, Q.Y. Feng, S.L. Zuo, Preparation characterization, and antibacterial activity of silver nanoparticle-decorated graphene oxide nanocomposite, ACS Appl. Mater. Interfaces 7 (2015) 6966–6973.
[24] S.N. Chen, X. Li, Y.Y. Zhao, L.M. Chang, J.Y. Qi, Graphene oxide shell-isolated Ag nanoparticles for surface-enhanced Raman scattering, Carbon 81 (2015) 767–772.
[25] J.J. Wang, G.P. Yin, H. Liu, Carbon nanotubes supported Pt-Au catalysts for methanol-tolerant oxygen reduction reaction: a comparison between Pt/Au and Pt Au nanoparticles, J. Power Sources 194 (2009) 668–673.
[26] H. He, H.B. Wang, K. Li, J. Zhu, J.S. Liu, X.D. Meng, X.S. Shen, X.H. Zeng, W.P. Cai, Green and yunable decoration of graphene with spherical nanoparticles based on laser ablation in water: a case of Ag nanoparticle/graphene oxide sheet composites, Langmuir 32 (2016) 1667–1673.
[27] Y. Wei, X. Zuo, X.Q. Li, S.S. Song, L.W. Chen, J. Shen, Y.D. Meng, Y. Zhao, S.D. Fang, Dry plasma synthesis of graphene oxide-Ag nanocomposites: a simple and green approach, Mater. Res. Bull. 53 (2014) 145–150.
[28] Y. Haldorai, B.K. Kim, Y.L. Jo, J.J. Shim, Ag@graphene oxide nanocomposite as an efficient visible-light plasmonic photocatalyst for thedegradation of organic pollutants: a facile green synthetic approach, Mater. Chem. Phys. 143 (2014) 1452–1461.
[29] H.Y. Wu, Y.H. Lai, M.S. Hsieh, S.D. Lin, Y.C. Li, T.W. Lin, Highly intensified surface enhanced Raman scattering through the formation of p,p '-imercaptoazobenzene on Ag nanoparticles/graphene oxide nanocomposites, Adv. Mater. 1 (2014).
[30] K.S. Hui, K.N. Hui, D.A. Dinh, C.H. Tsang, Y.R. Cho, W. Zhou, X. Hong, H.-H. Chun, Green synthesis of dimension-controlled silver nanoparticle–graphene oxide with in situ ultrasonication, Acta Mater. 64 (2014) 326–332.
[31] K. Shameli, M.B. Ahmad, W.M. Yunus, N.A. Ibrahim, Y. Gharayebi, S. Sedaghat, Synthesis of silver/montmorillonite nanocomposites using gamma-irradiation, Int. J. Nanomed. 5 (2010) 1067–1077.
[32] A.M. Golsheikh, N.M. Huang, H.N. Lim, R. Zakaria, One-pot sonochemical synthesis of reduced graphene oxide uniformly decorated with ultrafine silver nanoparticles for non-enzymatic detection of H_2O_2 and optical detection of mercury ions, RSC Adv. 4 (2014) 36401–36411.
[33] S. Wang, Y. Zhang, H.L. Ma, Q. Zhang, W. Xu, J. Peng, J. Li, Z.Z. Yu, M. Zhai, Ionic-liquid-assisted facile synthesis of silver nanoparticle-reduced graphene oxide hybrids by gamma irradiation, Carbon 55 (2013) 245–252.
[34] K. Hareesh, R.P. Joshi, S.S. Dahiwale, V.N. Bhoraskar, S.D. Dhole, Synthesis of Ag-reduced graphene oxide nanocomposite by gamma radiation assisted method and its photocatalytic activity, Vacuum 124 (2016) 40–45.
[35] K.C. Hsu, D.H. Chen, Microwave-assisted green synthesis of Ag/reduced graphene oxide nanocomposite as asurface-enhanced Raman scattering substrate with high uniformity, Nanoscale Res. Lett. 9 (2014).
[36] R.D. Martinez-Orozco, H.C. Rosu, S.W. Lee, V. Rodriguez-Gonzalez, Understanding the adsorptive and photoactivity properties of Ag-graphene oxidenanocomposites, J. Hazard. Mater. 263 (2013) 52–60.
[37] F.K. Liu, Y.C. Hsu, M.H. Tsai, T.C. Chu, Using γ-irradiation to synthesize Ag nanoparticles, Mater. Lett. 61 (2007) 2402–2405.
[38] Z.W. Xu, L. Chen, B.M. Zhou, Y.L. Li, B.D. Li, J.R. Niu, M.J. Shan, Q.W. Guo, Z. Wang, X.M. Qian, Nano-structure and property transformations of carbon systems under γ-ray irradiation: a review, RSC Adv. 3 (2013) 10579.
[39] L. Chen, Z.W. Xu, J.L. Li, Y.L. Li, M.J. Shan, C.H. Wang, Z. Wang, Q.W. Guo, L.S. Liu, G.W. Chen, X.M. Qian, A facile strategy to prepare functionalized graphene via intercalation, grafting and self-exfoliation of graphite oxide, J. Mater. Chem. 22 (2012) 13460.
[40] A. Abedini, A.R. Daud, M.A.A. Hamid, N.K. Othman, E. Saion, A review on radiation-induced nucleation and growth of colloidal metallic nanoparticles, Nanoscale Res. Lett. 8 (2013).
[41] H. Jin, L. Chen, K. Zheng, Z.W. Xu, J. Shi, B.M. Zhou, M.J. Shan, Y.L. Li, Super-high interlayer spacing of graphite oxide obtained by γ-ray irradiation in air, J. Mater. Sci. 49 (2013) 827–832.
[42] T.V.M. Sreekanth, M.J. Jung, I.Y. Eom, Green synthesis of silver nanoparticles, decorated on graphene oxide nanosheets and their catalytic activity, Appl. Surf. Sci. 361 (2016) 102–106.
[43] Z.X. Jiang, J.J. Wang, L.H. Meng, Y.D. Huang, L. Liu, A highly efficient chemical sensor material for ethanol: Al_2O_3/graphene nanocomposites fabricated from graphene oxide, Chem. Commun. 47 (2011) 6350–6352.
[44] K.N. Kudin, B. Ozbas, H.C. Schniepp, R.K. Prud'homme, I.A. Aksay, R. Car, Raman spectra of graphite oxide and functionalized graphene sheets, Nano Lett. 8 (2008) 36–41.
[45] M.D. Stoller, S. Park, Y.W. Zhu, J.H. An, R.S. Ruoff, Graphene-based ultracapacitors, Nano Lett. 8 (2008) 3498–3502.
[46] M. Cai, D. Thorpe, D.H. Adamson, H.C. Schniepp, Methods of graphite exfoliation, J. Mater. Chem. 22 (2012) 24992.
[47] K. Gotoh, T. Kinumoto, E. Fujii, A. Yamamoto, H. Hashimoto, T. Ohkubo, A. Itadani, Y. Kuroda, H. Ishida, Exfoliated graphene sheets decorated with metal/metal oxide nanoparticles: simple preparation from cation exchanged graphite oxide, Carbon 49 (2011) 1118–1125.
[48] D.C. Marcano, D.V. Kosynkin, J.M. Berlin, A. Sinitskii, Z. Sun, A. Slesarev, L.B. Alemany, W. Lu, J.M. Tour, Improved synthesis of graphene oxide, ACS Nano 4 (2010) 4806–4814.
[49] C.B. Shi, L. Chen, Z.W. Xu, Y.N. Jiao, Y.L. Li, C.H. Wang, M.J. Shan, Z. Wang, Q.W. Guo, Monitoring influence of chemical preparation procedure on the structure of graphene nanosheets, Physica E 44 (2012) 1420–1424.
[50] C. Antti, B. Lundberg, The molecular and crystal structure of diimidazole silver(I) nitrate, $Ag(C_3H_4N_2)_2NO_3$, Acta Chem. Scand. 25 (1971) 1758–1766.
[51] Y.K. Yang, C.E. He, W.J. He, L.J. Yu, R.G. Peng, X.L. Xie, X.B. Wang, Y.W. Mai, Reduction of silver nanoparticles onto graphene oxide nanosheets with N,N-dimethylformamide and SERS activities of GO/Ag composites, J. Nanopart. Res. 13 (2011) 5571–5581.
[52] G. Liu, Y.J. Wang, X.J. Pu, Y. Jiang, L.L. Cheng, Z. Jiao, One-step synthesis of high conductivity silver nanoparticle-reduced graphene oxide composite films by electron beam irradiation, Appl. Surf. Sci. 349 (2015) 570–575.
[53] J.C. Fan, Z.X. Shi, Y. Ge, J.L. Wang, Y. Wang, J. Yin, Gum arabic assisted exfoliation and fabrication of Ag–graphene-based hybrids, J. Mater. Chem. 22 (2012) 13764.

[54] G.T. Fu, L. Tao, M. Zhang, Y. Chen, Y.W. Tang, J. Lin, T.H. Lu, One-pot, water-based and high-yield synthesis of tetrahedral palladium nanocrystal decorated graphene, Nanoscale 5 (2013) 8007–8014.
[55] R. Yoksan, S. Chirachanchai, Silver nanoparticles dispersing in chitosan solution: preparation by γ-ray irradiation and their antimicrobial activities, Mater. Chem. Phys. 115 (2009) 296–302.
[56] T. Zhu, K.Y. Teng, J. Shi, L. Chen, Z.W. Xu, A facile assembly of 3D robust double network graphene/polyacrylamide architectures via γ-ray irradiation, Compos. Sci. Technol. 123 (2016) 276–285.
[57] S.H. Huh, X-ray diffraction of multi-layer graphenes: instant measurement and determination of the number of layers, Carbon 78 (2014) 617–621.
[58] A. Henglein, M. Giersig, Formation of colloidal silver nanoparticles: capping action of citrate, J. Chem. Phys. 103 (1999) 9533–9539.
[59] J. Belloni, Nucleation, growth and properties of nanoclusters studied by radiation chemistry, Catal. Today 113 (2006) 141–156.
[60] J. Li, C.Y. Liu, Ag/Graphene heterostructures: synthesis, characterization and optical properties, Eur. J. Inorg. Chem. 2010 (2010) 1244–1248.
[61] J.F. Shen, T. Li, M. Shi, N. Li, M.X. Ye, Polyelectrolyte-assisted one-step hydrothermal synthesis of Ag-reduced graphene oxide composite and its antibacterial properties, Mater. Sci. Eng. C 32 (2012) 2042–2047.
[62] C.Y. Qiu, H.Q. Zhou, H.C. Yang, M.J. Chen, Y.J. Guo, L.F. Sun, Investigation of n-layer graphenes as substrates for raman enhancement of crystal violet, J. Phys. Chem. C 115 (2011) 10019–10025.
[63] L.L. Zhang, C.L. Jiang, Z.P. Zhang, Graphene oxide embedded sandwich nanostructures for enhanced Raman readout and their applications in pesticide monitoring, Nanoscale 5 (2013) 3773–3779.
[64] C. Zhang, S.Z. Jiang, Y.Y. Huo, A.H. Liu, S.C. Xu, X.Y. Liu, Z.C. Sun, Y.Y. Xu, Z. Li, B.Y. Man, SERS detection of R6G based on a novel graphene oxide/silver nanoparticles/silicon pyramid arrays structure, Opt. Express 23 (2015) 24811–24821.
[65] W. Fan, Y.H. Lee, S. Pedireddy, Q. Zhang, T. Liu, X.Y. Ling, Graphene oxide and shape-controlled silver nanoparticle hybrids for ultrasensitive single-particle surface-enhanced Raman scattering (SERS) sensing, Nanoscale 6 (2014) 4843–4851.
[66] Y.B. Xie, Y.J. Meng, SERS performance of graphene oxide decorated silver nanoparticle/titania nanotube array, RSC Adv. 4 (2014) 41734–41743.
[67] N. Todorova, T. Giannakopoulou, N. Boukos, E. Vermisoglou, C. Lekakou, C. Trapalis, Self-propagating solar light reduction of graphite oxide in water, Appl. Surf. Sci. 391 (2017) 601–608.
[68] F. Li, Z.F. Yu, L.Y. Zhao, T. Xue, Synthesis and application of homogeneous Fe_3O_4 core/Au shell nanoparticles with strong SERS effect, RSC Adv. 6 (2016) 10352–10357.